Journal of
Materials Chemistry B

Materials for biology and medicine

Accepted Manuscript

This article can be cited before page numbers have been issued, to do this please use: A. Prabhakaran, N. K. Sarangi, C. Smith, R. A. Arellano-Reyes and T. E. Keyes, *J. Mater. Chem. B*, 2026, DOI: 10.1039/D6TB00152A.

ROYAL SOCIETY OF CHEMISTRY

rsc.li/materials-b

View Article Online
DOI: 10.1039/D6TB00152A

ARTICLE

Impact of Phospholipase A2 Hydrolysis on Triplet-Triplet Annihilation Upconversion Liposomes

Received 00th January 20xx,
Accepted 00th January 20xx

DOI: 10.1039/x0xx00000x

Amrutha Prabhakaran,[a,†] Nirod Kumar Sarangi,[a,†] Colm Smith, [a] Ruben Arturo Arellano Reyes [a] and Tia E. Keyes [a*]

Triplet-triplet annihilation upconverting (TTA-UC) liposomes are of emerging interest because of their potential bioapplications in biosensing/imaging and light driven therapeutic delivery. However, a potential challenge in-vivo is their stability, since liposomes are prone to enzymatic degradation. Here, for the first time, we examine the impact of phospholipase hydrolysis on TTA-UC in liposome. We applied a TTA-UC liposome integrating a BODPY charge transfer sensitizer and perylene emitter pairs within DOPC membrane that shows an intense upconverted blue emission under green excitation. Phospholipase A_2 (PLA_2) enzyme was applied as the phospholipase as it is ubiquitous in the body and upregulated in a number of conditions. Surprisingly, we observed that PLA_2 treatment resulted in only a relatively modest decrease in TTA-UC intensity on exposure of the liposome to enzyme. In the presence of imipramine, a competitive inhibitor of PLA_2, or absence of Ca^{2+} on which hydrolysis depends, the enzymatic action is inhibited and TTA-UC intensity is indistinguishable from that in enzyme-free solution. Characterization of Ca^{2+} dependent enzymatic activity, drug-based inhibition and impact of hydrolytic procucts on membrane packing were assessed at pore-suspended lipid bilayer using confocal-based fluorescence lifetime imaging (FLIM), fluorescence lifetime correlation spectroscopy (FLCS), and electrochemical impedance spectroscopy (EIS). In the absence of the inhibitor, FLIM and FLCS studies show that enzymatic lipid cleavage increases lipid packing and decreases membrane fluidity without significant damage to the bilayer. Thus, we conclude that decreased TTA-UC output is due to the the increased viscosity of the membrane on hydrolysis. Electrochemcial impedance confirm these observations where membrane admittance decreases in response to phospholipid hydrolysis inidicating tighter lipid packing of the membrane with hydrolytic product. Nanoscale imaging using atomic force microscopy (AFM) in liquid mode at a mica-supported lipid bilayer further confirmed that PLA_2 caused phospholipid hydrolysis in presence of Ca^{2+}, resulting in nanoscale pore formation, whereas in the absence of either Ca^{2+} or imipramine treated PLA_2 did not induce lipid hydrolysis. Overall, our findings provide a molecular basis for understanding enzymatic action in general at a liposome bilayer model and show, for the first time, the influence of enzyme hydrolysis on TTA-UC integrity and efficiency in liposome.

1. Introduction

Triplet-triplet annihilation upconversion (TTA-UC) is a photophysical process in which two triplet sensitizer molecules, excited by low-energy (long-wavelength) light, transfer energy to triplet acceptor molecules. Upon mutual collision, the excited acceptors then undergo an annihilation reaction, promoting one molecule to the excited singlet state while the other relaxes to the ground state.[1–5] This excited acceptor fluoresces, emitting a photon at a higher frequency (higher energy) than the excitation originally used to initiate the process. [6–9]

TTA-UC is gaining traction as a route to light induced activation in processes such as photoactivated drug release and bioimaging because it offers the opportunity to use long wavelength, tissue-penetrating light to generate higher energy photons locally.[10–13] A promising approach to applying TTA-UC *in vivo* is via encapsulation of the dye system within liposomes. Liposomes are not only biocompatible drug delivery vehicles but also, an effective scaffold for TTA-UC; by confining the dyes to the two-dimensional (2D) space of the lipid bilayer, they increase collision probability and can significantly boost upconversion efficiency, depending on conditions.[5,14]

There have been a number of TTA-UC liposomal systems reported. For example, using palladium tetraphenyltetrabenzoporphyrin complex as photosensitizer and perylene as the annihilator, within giant unilamellar vesicles (GUVs) composed of either DOPC or DMPC, Askes et al., were used to image the membrane under red-to-blue light upconversion.[15] Exploiting large unilamellar vesicles (100 nm diameter) of DOPC, DMPC, and DSPC etc. Poznik et al., studied TTA-UC upon reconstituting platinum porphyrin PtOEP and an amphiphilic derivative of tris-(bipyridine) ruthenium (II) as photosensitizers and lipophilic diphenylanthracene as annihilator.[16] The reconstitution and selection of membrane composition and its intrinsic fluidity are as important for

[a] School of Chemical Sciences and National Centre for Sensor Research, Dublin City University, Dublin 9, Ireland. Corresponding author email: tia.keyes@dcu.ie
† These authors equally contributed to this work.
Electronic Supplementary Information (ESI) available: Experimental methods of substrate fabrication and additional FLIM, FCS and Laurdan Fluorescence data are presented. See DOI: 10.1039/x0xx00000x

View Article Online
DOI: 10.1039/D5TB01524A

efficient TTA-UC as the sensitizer-annihilator selection. Recently, we reported that a more fluidic liposomal membrane (low viscosity environment) leads to more efficient TTA-UC than a high viscosity membrane due to higher probability of collision between sensitizer and annihilator, which is crucial when designing a model for bioimaging.[5] We also demonstrated that the relative orientation of the sensitizer and annihilator (B2PI-perylene) within the lipid bilayer is a critical factor for efficient TTA-UC.[14]

Overall, therefore, liposomal TTA-UC is nowwell established, but for most reported systems, in vivo/vitro biological applications are the ultimate aim, and an important consideration that has not been addressed to date is if enzymatic activity impacts TTA-UC within such systems.[5] The cellular environment contains endogenous enzymes that target phospholipids that may impact the liposome or indeed disrupt it.[17–19] Indeed for liposomes, enzymatic reaction, has been shown to influence membrane fluidity and phase.[20] Because lipid membrane fluidity is a key modulator of liposomal TTA-UC, changes in fluidity pertaining to phospholipase action and its hydrolytic product may be important considerations in the design of liposomal TTA-UC systems for in-cellulo or in vivo application (Scheme 1). Furthermore, enzymatic alterations to TTA-UC may be an interesting way to build logic-gated TTA-UC e.g. for drug delivery. To our knowledge these questions have not been explored to date.

Phospholipid degradation is an essential process in phospholipid metabolism that occurs in all living organisms. It plays a structural role, for example, in membrane modelling and also serves in specific signalling pathways.[21,22] Phospholipase enzymes are responsible for phospholipid degradation and, they are found throughout the body as both extracellular and intracellular phospholipases. The latter are prevalent at cell membranes and within the lysosome and Endoplasmic reticulum (ER).[23] Phospholipase A_2 (PLA_2) are a sub-group of phospholipase enzymes that specifically catalyze the hydrolysis of the sn-2 ester bond in phospholipids, releasing fatty acids such as arachidonic acid (AA) and docosahexaenoic acid (DHA) that on further reaction with oxygenases such as COX, form eicosanoids and docosanoids. These are signalling molecules involved in inflammation, pain, immunity, and cell growth. PLA_2 overexpression has been linked to the development and spread of cancers including notably gastrointenstinal, colon, breast and prostate cancers.[24–26] Thus PLA_2 are of significant biomedical interest. Physiological concentration of phospholipase seems to varies with intracellular location and tissue type ranging from nanomolar to 100s of nanomolar in activated tissues. [24–26]

Since PLA_2 degrades the liposomal phospholipids into *sn*-1-ether lysophospholipids, this is expected to alter or perhaps even destroy TTA-UC function in TTA-UC liposomes.[27–30, 30–33] This is explored in this report for the first time, where we examine the impact of PLA_2 enzymolysis on TTA-UC in a liposomal system and unravel the PLA_2 mediated membrane organization, underlying phospholipase kinetics, role of Ca^{2+} and inhibition on the system. We apply an optimised and well characterised TTA-UC liposomal system developed by us to this study. This comprises of DOPC liposomes with 1: 10 ratio of an iodinated BODPY sensitizer with perylene annihilator (Figure S1).[4,5,7] We have described how high fluidity of the DOPC membrane is essential in TTA-UC as efficient diffusion supports collision between the constituents leading to efficient TTA-UC. But also as DOPC is unsaturated and froms homogenous L_D phase liposomes, they are likely to be a particularly vulnerable composition and so offer a good model system to study phospholipid degradation.

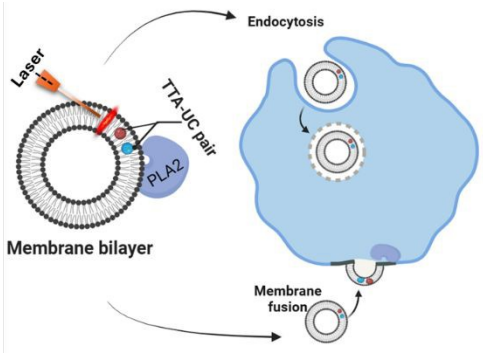

Scheme 1 Schematic illustration of TTA-UC pair embedded in liposomal membrane bilayer (left) nanocarrier and its different route for cell membrane uptake- Image was created using BioRender and PowerPoint.

To support our study we also apply a microcavity based pore-suspended lipid bilayer (MSLB) as a multimodally accessible tool to directly evaluate the impact of PLA_2 on DOPC membrane fluidity using fluorescence lifetime correlation spectroscopy, fluorescence lifetime imaging, and label-free electrochemical impedance spectroscopy.

2. Materials and methods

2.1 Materials

Ph-Bodipy-2-perylene-Iodine (B2PI, Fig S1, SI) was synthesized according to the protocol described in Reyes et al.[4] Perylene and PLA_2 were purchased from Sigma Aldrich. 1,2-dioleyl-*sn*-glycerophosphocholine (DOPC) in powder form was purchased from Avanti polar lipids. 1,2-dioleoyl-*sn*-glycero-3-phosphoethanolamine labelled ATTO655 (DOPE-ATTO655) and ATTO532 (DOPE-ATTO532) was purchase from ATTO-TEC GmbH (Siegen, Germany). Polydimethylsiloxane silicon elastomer (PDMS) was purchased from Dow Corning GmbH (Wiesbaden, Germany). Gold disk electrodes consisting of silicon wafers coated with a 100 nm layer of gold on a 50 Å layer of titanium adhesive were obtained from AMS Biotechnology Inc. Monodisperse polystyrene latex spheres of different sizes were obtained from Bangs Laboratories Inc. The commercial cyanide free gold plating solution (TG-25 RTU) was obtained from Technic Inc. All other HPLC grade reagents were obtained from Sigma-Aldrich and used as obtained. Ultra-pure water with a resistivity 18.2 MΩcm was produced by a Milli-Q (Millipore Academic) system and used for buffer preparation. Tris-HCl buffer was prepared using trisaminomethane, purchased from Sigma-Aldrich to a final concentration of 0.1 M and the pH was

View Article Online
DOI: 10.1039/D5TB01624A

adjusted to 7.4 using HCl. 0.1 M NaCl was also added, and the buffer was stored in refrigerated conditions.

2.2 Fabrication of gold and PDMS microcavity array

Polystyrene (PS) microsphere lithography was used to fabricate both gold and PDMS microcavity array electrodes, as reported previously.[31–33] Detailed preparation method is given in the ESI.

2.3 Liposome preparation

Large unilamellar vesicles (LUV) or liposomes were prepared by the hydration extrusion method.[34,35] The DOPC lipid dissolved in chloroform was mixed with the desired concentration of photosensitizer and annihilator or with 0.01% DOPE-ATTO655 in a 1.5 mL vial. The solvent was evaporated under N_2 flow further dried by putting the reaction vial in vacuo for 30-60 minutes. The resulting thin lipid film was hydrated with 1 mL Tris-HCl buffer followed by 60 s of vortexing to mix the solution thoroughly. The solution was extruded through a polycarbonate membrane of 100 nm pore size a minimum of 11 times. The hydrodynamic diameter of the resulting liposomes was measured by dynamic light scattering in a Malvern Zetasizer Ultra instrument. The vesicle solutions were stored at 2 °C and used within 3 weeks of preparation.

2.4 Fabrication of microcavity suspended lipid bilayers

The assembly of lipid bilayer spanned across the aqueous filled microcavity array, both gold and PDMS array substrates were completed as described previously and explained in ESI by using a combination of Langmuir-Blodgett transfer followed by vesicle fusion (LB-VF) method.

2.5 TTA-UC Measurements

The TTA-UC measurements were carried out using Varian Cary Eclipse fluorescence spectrophotometer using a 532 nm diode laser of 10 mW power (Edmund Optics) as excitation source with 1 mm diameter beam and 1.27 Wcm^{-2} power density. The TTA-UC measurements were performed by blocking the excitation line in bioluminescence measurement mode. The upconverted emission measurements in liposomes were carried out by N_2 purging the sample in a quartz cuvette of 1 cm pathlength. Upconversion quantum yield and threshold power density measurements were carried out on an Edinburgh Instruments FS5 Spectrofluorimeter as previously reported.[14] To activate the enzyme, calcium chloride dihydrate was added to the liposome solution and incubated for 15 minutes. The upconverted emission was recorded across the range 400 to 500 nm to avoid the interference from the excitation source.

2.6 Electrochemical Impedance Spectroscopy

Electrochemical measurements were performed with a CH760A potentiostat (CH Instruments, USA). A standard 3-electrode cell was used comprised of gold microcavity suspended bilayer as working electrode, an Ag/AgCl (1 M KCl) reference electrode and a platinum wire auxiliary electrode. The EIS data were measured over a frequency range of 0.05 to 10^5 Hz with an AC modulation amplitude of 0.01 V at a potential DC bias of 0 V (vs Ag/AgCl). All measurements were carried out in a glass cell (approximate volume of 4 mL) in contact with Tris-HCl buffer maintained at pH 7.4. The EIS of the aqueous filled microcavity array coated with the lipid bilayer was measured initially prior to the addition of PLA_2 to ensure signal stability on initial contact with the electrochemical cell/ Tris-HCl buffer at 0 V an initial fluctuation of resistance is seen that equilibrates within an hour and then remains unchanged over a prolonged window (24 hrs). Therefore, an equilibration time of 60-90 mins was allowed for all EIS cells following which an additional 30 minutes was allowed for incubation of Ca^{2+} prior to the addition of PLA_2. Each EIS measurement takes approximately 4 min and was carried out at room temperature (22±1 °C). The measured data were analysed using Z-View software applying the equivalent circuit fitting model (ECM) that was established and tested previously as a good model for the MSLB.[36] Using this approach we can estimate membrane resistivity and capacitance values before and after PLA_2 binding. The circuit consists of a parallel combination of solution resistance (R_s) and capacitor in series with a parallel combination of constant phase element, CPE (C_{array}) and a cavity resistive element (R_{array}) of the microcavity array, and the membrane is approximated by a resistive element (R_M) in parallel with a CPE (Q_M). A Constant Phase Element (CPE) is used in the equivalent circuit instead of pure capacitors as the impedance of solid electrodes usually deviates from pure capacitor due to microscopic chemical inhomogeneity on both the electrode surface and in the lipid bilayer. Depending on the composition, as described below, from EIS, the bilayer resistance for an intact bilayer ranges from 2 to 10 MΩ (compared to kΩ resistance of SAM modified cavity array prior to bilayer deposition). We have previously shown that this resistance range corresponds to an intact SLB and so used the resistance values to validate the bilayer prior to measurement.[37]

2.7 Fluorescence lifetime imaging and fluorescence lifetime correlation spectroscopy

Fluorescence lifetime imaging (FLIM) and fluorescence lifetime correlation spectroscopy (FLCS) experiments were performed using a MicroTime 200 system (PicoQuant GmbH, Germany) consisting of FCS module, dual SPD detection unit, time-correlated single photon counting (TCSPC), and inverted microscope model Olympus X1-71 with an Olympus UPlan SApo 60×/1.2 water immersion objective. Before FLIM, reflectance images were collected using an optical density (OD3) filter which assesses the buffer filled cavities. The fluorescently labelled lipid probe DOPE-ATTO655 was excited using pulsed picosecond lasers at 640 nm LDH-P-C-640B. A single mode optical fibre guides the laser to the main unit and provides a homogeneous Gaussian profile. The laser was pulsed at 20 MHz, corresponding to an interval of 50 ns. The emitted fluorescence was collected through the same microscope objective and dichroic mirror z532/635rpc blocked the back scattered light and HQ670lp AHF/Chroma filter for 640 nm was used to clean up the signal. Fluorescence was detected using a single photon avalanche diode from MPD (PicoQuant). The TCSPC system (PicoHarp 300 from PicoQuant) enabled simultaneous

assessment of the lifetime in a nanosecond range along with the time of diffusion in the millisecond range. A 50 µm pinhole was used to confine the volume of detection in the axial direction whilst blocking all off-focal-plane light.

Spatially resolved, point fluorescence lifetime correlation spectroscopy measurements were carried out at microcavity supported lipid bilayer membranes (MSLB), supported across porous PDMS substrates, according to a method previously described.[38,39] Measurements were collected focussing on membrane membrane suspended across the centre of cavities. The upper leaflet of the bilayer was doped with 0.01 mol% of fluorescent label; DOPE-ATTO655. Point FLCS measurements were then recorded for 30 s per cavity, with an average of 40-50 cavities for each autocorrelation function (ACF) for each bilayer and enzyme type. All measurements were recorded at room temperature 20±0.4 °C. The fluorescence fluctuation intensity is multiplied by a time shifted replica of varying values (lag time, τ) and the temporal averages yields the ACF, G (τ) for the respective lag time. The ACF obtained from the bilayer spanned over 2D PDMS array is fitted using eq. (1).

$$G_{2D}(\tau) = \frac{1}{N}\sum_{i=1}^{m}\left(1+\left(\frac{\tau}{\tau_{Di}}\right)^{\alpha}\right)^{-1} \qquad (1)$$

where, τ_{Di} is the translational transit time of the ith fluorescent diffusing species in and out of the confocal volume, α is anomalous coefficient, which deviates from 1 if the diffusion does not follow normal Brownian motion. From the transit time, the diffusion coefficient (D) was determined using eq. (2),

$$D = \frac{\omega^2}{4\tau_D} \qquad (2)$$

where, ω is the waist diameter of the confocal beam determined as 1/e^2 of 0.135 and obtained by calibrating the microscope system with an aqueous solution of ATTO655 with known diffusion coefficient value diffusing freely in 3D.

3. Results and discussion

3.1 TTA-UC results

To understand the impact, if any, phospholipase A_2 (PLA_2) enzymatic hydrolysis has on TTA-UC efficiency in a liposomal formulation, as described we used a recently established system. This comprised of 0.5 µM B2PI and 5 µM perylene as the TTA-UC pair within DOPC liposomes. This system was previously optimised and upon 532 nm laser excitation, yields a strong anti-Stokes emission due to perylene with peaks at 444 nm and 474 nm (Figure S2a, SI).[4,5,7] In our previous report, TTA-UC at DOPC liposomal membranes was studied in PBS. In the present study, since PLA_2 enzymatic activity is dependent on the presence of Ca^{2+}, we used Tris-HCl (pH 7.4) buffer to avoid Ca^{2+} complex formation with phosphate anion this buffer. Ca^{2+} is soluble and stable in Tris-HCl.

Control experiments were first performed to establish if Ca^{2+} ion influences TTA-UC in the liposome. In the presence of 5 mM Ca^{2+}, no statistically significant impact on the upconversion quantum yield (QY) of the system was observed (Fig. 1a). Upconversion intensity increased modestly, however, by about 10% (Fig. S2a, red (SI)) compared to liposome in buffer alone (black, Fig. S2a (SI)). Ca^{2+} is thought to preferentially associate with the negatively charged phosphate groups in the membrane headgroup region. This interaction leads to ion-lipid-ion bridges that dehydrate the bilayer surface headgroup through a water squeeze-out mechanism, which likely accounts for the small rise in UC intensity observed.[40]

Next, 5 µM PLA_2 was added to the liposome solution and TTA-UC QY measured at time intervals of 10, 30 and 60 min. In mammalian cells PLA2 is usually present in the We used 5 µM PLA_2 in these studies as this exceeds the upper end of the physiological range to ensure the response was the most that could be expected in the physiological system.[41] As shown in Figure 1a, enzyme action caused a decrease in TTA-UC quantum yield but by 60 mins, the changes to had stabilised at ~50% with no further change observed over extended studies of 3 hours. The threshold upconversion intensity was measured before and after incubation with PLA_2 (Figure 1b) and was observed to increase from 22 mW/cm^2 to 57 mW/cm^2. The stability of liposomes under these enzymatic conditions was confirmed by dynamic light scattering, as detailed below.

Given the water insolubility of the sensitizer and annihilator it is very unlikely that dye expulsion is the cause of the TTA-UC decrease observed. Rather, the hydrolysis of PLA_2 is believed to modify the packing of lysophospholipids and fatty acid catalytic product of DOPC. This is expected to influence the lipid mobility and potentially also phase, potentially altering both upconversion quantum yield and threshold power intensity. To investigate this, we determined the diffusion coefficient of the lipid in relation to enzyme treatment in the next section (vide infra).

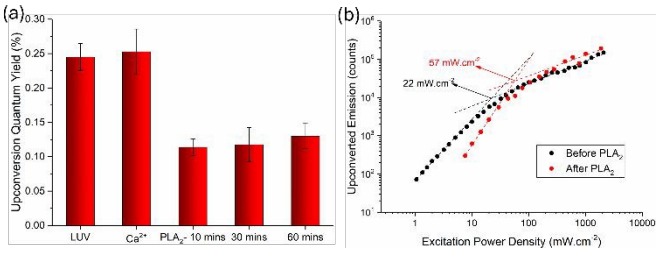

Fig. 1 (a) Upconversion quantum yields from DOPC liposomes incorporated with 0.5 µM B2PI and 5 µM perylene before and after the addition of 5 mM Ca^{2+} and after the subsequent addition of 5 µM PLA_2 measured at 10, 30 and 60 minutes (N=3). (b) Threshold upconversion intensity before and after addition of PLA_2. All liposomes are in deaerated Tris-HCl buffer of pH 7.4 and all TTA-UC experiments are carried out in presence of 20 mM sodium sulphite as an O_2 quencher. All samples were excited with a 532 nm CW laser.

We also confirmed that the changes to TTA-UC are not due to PLA_2 interaction with membrane in absence of enzyme activity. To that end, the upconversion emission was measured in presence of PLA_2 (5 µM) but in the absence of Ca^{2+}. Under these conditions, TTA-UC intensity did not change, indicating that enzyme hydrolysis is responsible for TTA-UC reduction (Figure

View Article Online
DOI: 10.1039/D5TB00153A

2b, SI). This observation also adds to the growing body of evidence that Ca^{2+} is necessary for PLA_2 catalytic action.[42,43] We then investigated the effect of imipramine, a small molecule inhibitor of PLA_2, on TTA-UC. After incubating 20 μM of imipramine with 5μM of PLA_2, the solution was added to the liposomal solution containing Ca^{2+}. Figure 2a shows representative data, that reveal upconversion emission does not diminish when catalytic activity of PLA_2 is blocked. This again indicates that lipid hydrolysis is responsible for TTA-UC modification.

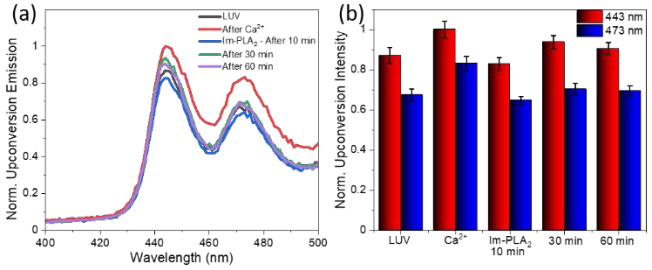

Fig. 2 (a) Normalised TTA-UC emission spectra from DOPC liposomes incorporated with 0.5 μM B2PI and 5 μM perylene before (black) and after (red) the addition of 5 mM Ca^{2+} and after the addition of 5 μM PLA_2 pre-incubated with 20 μM imipramine measured at 10, 30 and 60 minutes. (b) Corresponding intensity histogram of each spectrum in panel (a). All liposomes are in Tris-HCl buffer of pH 7.4, and measured in triplicates (N =3). All TTA-UC experiments are carried out in presence of 20 mM sodium sulphite as an O_2 quencher.

In the presence of the inhibitor, modest increases in upconversion emission intensities are observed over time, although change is not systematic (Figure 2b). Such variation is not observed in a control where stable TTA-UC output was observed over time without the addition of any reagent. This change is likely due to the impact of imipramine on the membrane itself which has been shown previously to modestly increase the membrane fluidity. To confirm this we completed a control FLCS experiment applying imipramine to DOPC bilayer where we did observe a modest but significant decrease (4.1±0.3 $\mu m^2 s^{-1}$) in DOPC fluidity (Figure S9).[39]

3.2 Dynamic light scattering (DLS) studies of PLA_2 action

Dynamic light scattering (DLS) was conducted to determine the effect, if any, that the interaction between PLA_2 and liposomes has on the liposomes' size and integrity. In the absence of PLA_2, the average DOPC liposome diameter, (containing B2PI and perylene) was 120±5 nm in Tris-HCl buffer, pH 7.4 (Figure S3a, SI). In the absence of Ca^{2+}, the liposome solution remained homogeneous and exhibited an unaltered, unimodal size in the presence of PLA_2(Figure S3b, SI). However, after PLA_2 treatment in presence of Ca^{2+}, the particle size distribution becomes bimodal. As shown in Figure S3c (SI), the liposomes of 120±5 nm diameter remain, but in addition, a new species with average diameter of 760 nm appears, and the solution becomes somewhat turbid. Though the size dispersity, reflected in the full width half maximum (FWHM) of the size distribution was found to become narrower on PLA_2 activity as compared to when there is no activity of PLA_2. Conversely, the particle size distribution of liposome in contact with Ca^{2+} and PLA_2, that has been previously treated with imipramine also (Figure S3d, SI), remains unchanged with a diameter of 120±5 nm. It has been shown across multiple studies on enzyme responsive liposomes in drug delivery, that enzyme treatment causes increase to liposome diameter in DLS and alters size distributions of products. This has been attributed to changes in the lipid packing and also liposome fusion induced by lipid hydrolysis, leading to liposome aggregation.[44–46] Our data are strongly consistent with these reports, including the magnitude of the dimension changes that we observe.

Next, to understand the impact of PLA_2 on DOPC membrane properties we conducted analysis using microcavity supported lipid bilayers (MSLB), a true biomimetic model membrane suitable for multimodal surface-sensitive interrogation, which are not accessible for liposome. We employed single-molecule fluorescence lifetime imaging, fluorescence correlation spectroscopy, and electrochemical impedance to elucidate PLA_2's effects on the DOPC membrane.

3.3 Fluorescence lifetime imaging (FLIM) and fluorescence lifetime correlation spectroscopy (FLCS) studies on PLA_2 catalysed hydrolysis of DOPC membrane.

The decrease in TTA-UC intensity observed on PLA_2-induced lipid hydrolysis is likely due to changes in packing order of membrane. Presumably, this occurs rather than complete membrane disruption since the latter would be expected to eliminate TTA-UC. To confirm this hypothesis, we examined the impact of PLA_2 on membrane properties using fluorescence lifetime imaging (FLIM) and fluorescence lifetime correlation spectroscopy (FLCS). We used micropore-suspended lipid bilayers (MSLB) over optically transparent PDMS to model membrane behaviour on PLA2 hydrolysis as it allowed us to directly interrogate the impact of PLA_2 catalysis on DOPC membrane organization and diffusivity/viscosity.

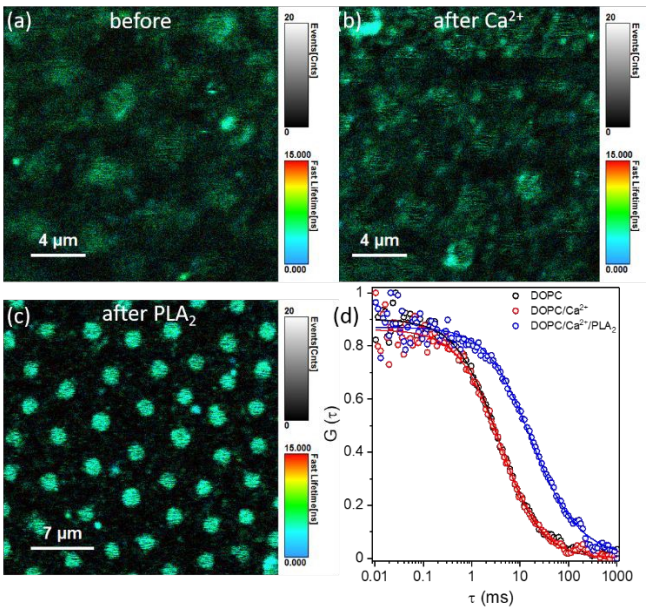

View Article Online DOI: 10.1039/D6TB00153A

Fig. 3 Fluorescence lifetime images (FLIM) of DOPC MSLBs labelled with 0.01 mol% DOPE-ATTO655 (upper leaflet) (a) before, (b) after the addition of 5 mM Ca^{2+}, and (c) after the addition of 5 μM PLA_2 in presence of Ca^{2+}. (d) Representative FLCS autocorrelation functions of DOPC MSLB labelled with 0.01 mol% DOPE-ATTO655 (upper leaflet) before (open black), after 5 mM Ca^{2+} addition (open red) and after the addition of 5 μM PLA_2 in presence of Ca^{2+} (open blue). FLCS data were collected from 40-50 cavities and the average is shown. The solid lines are the 2D diffusion fit using equation 1. The scale bar in each panel is 4 μm. All measurements were carried out in Tris-HCl buffer at pH 7.4.

Figure 3a shows representative FLIM images of DOPC MSLB supported over PDMS microcavity array filled with Tris-HCl buffer. To visualize the bilayer, the upper leaflet of DOPC bilayer was doped with 0.01 mol% fluorescent dye labelled lipid; DOPE-ATTO655. The membrane was prepared via the Langmuir Blodgett-vesicle fusion (LB-VF) method, as detailed in experimental section, and the MSLB was sealed within a microfluidic flow chamber that permits introduction of reagents to the contacting solution at the outer leaflet of the array. Buffer filled cavities upon which bilayer is spanned are shown in the reflectance image (Fig. S5a, SI). Upon addition of 5 mM Ca^{2+}, some lateral heterogeneity becomes evident in the FLIM image indicating some reorganization of membrane (Figure 3b), notwithstanding the diffraction limit of the method, that prevents visualisation of nanoscale reorganisation. Upon addition of PLA_2, the overall molecular brightness increased (Figure 3c). Figure 3d shows representative autocorrelation function (ACF) traces for the DOPC bilayer in the absence (open black), in the presence of 5 mM Ca^{2+} (open red), and in the presence of both Ca^{2+} and PLA_2 (open blue). The solid lines in panel 3d show the fit to the 2D diffusion model, as described in equation 1. All FLCS measurements were performed at the bilayer plane by positioning the FLCS observation volume at the centre of the cavity-spanning bilayer, ensuring that the free-standing bilayer was measured without interference from the surface. The diffusion coefficient obtained from DOPC bilayer was determined as 10.1±0.2 $\mu m^2 s^{-1}$, in agreement with previous reports in both MLSB and giant unilamellar vesicle (GUV).[47] Upon Ca^{2+} addition, the lipid diffusivity reduced to 9.3±0.17 $\mu m^2 s^{-1}$. Upon further addition of 5 μM PLA_2, post 30 min incubation, the lipid diffusivity reduced dramatically to 1.4±0.3 $\mu m^2 s^{-1}$. This indicates a marked increase in membrane viscosity upon treatment with the enzyme. In all FLCS experiments both before and after Ca^{2+} and PLA_2 treatment, the anomalous coefficient (α) remained 1, indicating Brownian diffusion was preserved. To further investigate microviscosity changes of the DOPC bilayer in response to enzyme, we conducted Laurdan fluorescence spectroscopy in Tris buffer (dotted line) and from DOPC LUV (black solid line) with and without PLA_2 in the presence of Ca^{2+} (Fig. S4a, SI). The fluorescence spectrum of Laurdan from DOPC LUV remains virtually same with the addition of Ca^{2+}. However, in the presence of both Ca^{2+} and PLA_2, there is a notable increase in fluorescence emission intensity at 430 nm and a corresponding drop at 490 nm. In the presence of PLA_2, the generalized polarization (GP) value (equation S1, SI) significantly increased from -0.18 to -0.07 (Fig. S4b, SI), consistent with our FCS findings at the MSLB, this indicates PLA2/Ca^{2+} enhanced membrane ordering/viscosity.

In a control experiment, when PLA_2 was added to the DOPC membrane in the absence of Ca^{2+}, the molecular brightness from FLIM did not change (Fig. S5b and c, SI) compared to that of FLIM image when Ca^{2+} was present (Figure 3b and c). Most notably lipid diffusivity after PLA_2 incubation was reduced modestly to 8.5±0.22 $\mu m^2 s^{-1}$ as shown in Figure S5d (red) when Ca^{2+} was not present, in contrast to the dramatic decrease observed when both Ca2+ and PLA_2 are jointly present. The lifetime value obtained from the pore-spanning membrane (number of pores analysed = 8) increased barely from 3.15±0.003 ns to 3.23±0.004 ns (Figure S6, SI). These relatively minor changes sugest some physisorption of PLA_2 is occurring at the bilayer surface in the absence of Ca^{2+}. However, our data indicate that both Ca^{2+} and PLA_2 must be present to stimulate enzymatic action, and that membrane lipid hydrolysis leads to a gross increase in in membrane viscosity.[48,49] The fact that the DOPC membrane viscosity increases so significantly during hydrolysis is surprising and suggests that phase changes occur in the membrane, yet there is no fundamental loss of the membrane structural integrity because TTA-UC is retained. The observation is consistent with a report by Leidy et al. who showed that DMPC gel-phase membranes underwent a profound phase change during PLA_2 enzymolysis while retaining membrane integrity.[50]

The decrease in TTA-UC we observe is likely due to this reduced lateral diffusivity, which decreases collision frequency of the annihilator and sensitizer as reported in more viscous/gel phase lipsosmes, though phase partitioning may also play a role. We saw no evidence from spectroscopic studies for loss of annihilator and sensitizer from the membrane and this is deemed unlikely anyway as they are not water soluble.

We next examined the impact of PLA_2 inhibitor on membrane organization. Imipramine is an inhibitor of PLA_2 and when the enzyme was pre-treated with this reagent, prior to its incubation with the DOPC MSLB in the presence of Ca^{2+}, the FLIM images (Figure 4c) were indistinguishable from those of the pristine DOPC MSLB without (Figure 4a) or with Ca^{2+} (Figure 4b). Figure 4d compares ACF traces before (black), after Ca^{2+} (red) and after imipramine treated PLA_2 (green) incubation. The membrane diffusivity after 30 min of incubation with PLA_2 treated imipramine is recorded as 4.1±0.3 $\mu m^2 s^{-1}$, which is significantly reduced compared to the pristine DOPC membrane. However, the effect is much reduced in comparison to PLA_2 incubation (1.4±0.3 $\mu m^2 s^{-1}$). Assuming imipramine is effective as an inhibitor for the hydrolytic action of PLA_2, the resulting viscosity change may be due to adsorption of the of imipramine-PLA_2 at the membrane surface, leaving the membrane viscous; such effects have been noted previously on membrane-protein adsorption. This is consistent with our upconversion emission data (vide infra). The FLIM images of imipramine treated PLA_2 (Fig. 4c) are also consistent with this model, since they show no evidence of physical changes such as domain formation at the membrane or any increase in molecular brightness that we observed in the inhibitor free enzyme hydrolysis (cf. Fig. 3c). Likewise, the fluorescence lifetime values of labelled lipids in the imipramine/PLA_2 treated

membrane did not change when compared to the pristine membrane (Fig. S7, SI).

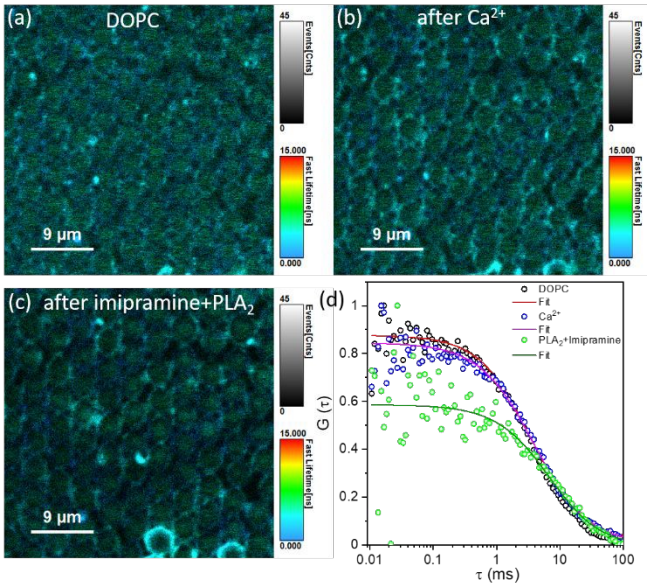

Fig. 4 Fluorescence lifetime images (FLIM) of pristine DOPC MSLB (a) before, and after addition of (b) 5 mM Ca^{2+}, and (c) PLA_2 pre-incubated with imipramine in presence of Ca^{2+} taken at the identical regime. The concentration of imipramine and PLA_2 were 20 µM and 5 µM respectively. In each case in panel b and c, the images were acquired following 30 minutes of incubation. (d) ACF traces obtained from pristine bilayer (open black) before, after Ca^{2+} (open blue) and after PLA_2 treated imipramine (open green) further spanned over PDMS microcavity array filled with Tris-HCl buffer. The scale bar in each panel is 9 µm. The solid lines are the 2D diffusion fit using equation 1.

3.4 Electrochemical impedance studies of lipid hydrolysis using PLA_2

Electrochemical impedance of lipid bilayers is highly sensitive to lipid packing, pore formation and membrane remodelling; therefore, we complimented our photophysical studies with electrochemical impedance spectroscopy (EIS) of PLA_2 action on DOPC membranes. In EIS, the important parameters to consider are membrane resistance and capacitance, which show how the modification of membrane impedance characteristics is affected by PLA_2 activity both in the presence and absence of Ca^{2+} over time. The capacitance characteristics of a lipid bilayer are related to the thickness of the membrane, and non-Faradaic EIS often makes use of alternating current (AC) at different frequencies to evaluate the resistance to ionic conduction through the bilayer. Macromolecular (here PLA_2) binding at the membrane interface, can result in thickening of the membrane or increase in packing order of membrane, which is marked by a decrease in capacitance and an increase in resistance; yet, the integrity of the membrane is not compromised. A rise in membrane capacitance with accompanying resistance decrease, on the other hand, suggests membrane degradation or thinning due to membrane damage or decrease in packing order. In contrast, a decrease in resistance with no change in capacitance is indicative of nanoporation within the membrane.[51,52] These parameters can be derived from the EIS data by fitting with appropriate equivalent circuit model (ECM).

In our EIS experiments, a DOPC bilayer was suspended over a gold microcavity imprinted array analogous to that used for FLCS studies. Hexagonally packed microcavity array (1 cm×1 cm), with each pore diameter 1 µm and pore depth 0.5 µm imprinted array was fabricated over gold coated silicon chips by soft-lithography method using 1 µm polystyrene sphere, according to our established protocols.[52–54]

View Article Online DOI: 10.1039/D6TB00152A

Microcavity suspended lipid bilayers (MSLBs) over gold microcavity imprinted array were prepared via the LB-VF method used for the PDMS arrays. The MSLB serves as the working electrode in a custom-built cell of 3 to 4 mL volume. The electrolyte was Tris-buffer, pH 7.4. A typical non-Faradaic Nyquist and angular frequency normalized complex capacitance plot of bare cavity (black square) and DOPC MSLB EIS data are shown in Figure 5 a and b respectively. The Nyquist traces as semicircle arcs represents the real (Z') and imaginary (Z'') parts of the complex impedance, which originate from the resistance and capacitance of the electrochemical cell. When compared to the bare cavity or bilayer-free electrodes (black square, Figure 5a), the non-Faradaic Nyquist trace of a DOPC spanned MSLB (red circle) shifts more towards -Z″ (y-axis), indicating an increase in impedance of the membrane due to the presence of dielectrics (here lipid bilayer membrane). It is worth noting that the presence of mercaptohexanethiol SAM only slightly increases the impedance compared to the bare cavity array, because the thiol molecules are spatially restricted to the pore interstitial regions on the top surface of the array. The angular frequency normalized complex capacitance plots (-Y″/ω vs Y′/ω, where Y is the electrode admittance and ω is the angular frequency) can provide a direct visualization membrane capacitance property. Typically, the complex capacitance plots (Figure 5b) are semi-circular and indicate near-ideal behaviour for DOPC MSLB. The diameter of the high frequency semicircle on the imaginary axis is proportional to the magnitude of the bilayer capacitance. As seen from Figure 5b, the capacitance of a bare gold array electrode (black square) decreases by one-fold

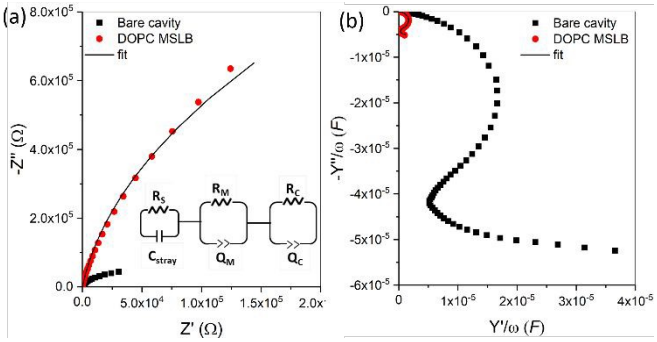

Fig. 5 Representative non-Faradaic (a) Nyquist (-Z'' vs Z') and (b) angular frequency normalized complex capacitance (-Y''/ω vs Y'/ω) plots of bare cavity (black square) and cavity spanned DOPC MSLB (red circle). Inset in panel a shows the equivalent circuit model used to fit the EIS data. Solid wine lines in panel a,b are the corresponding fit. All EIS measurements are performed in Tris-HCl of pH 7.4 buffer at 0 V bias potential with an A.C amplitude of 10 mV within a frequency range of 0.05 Hz and 10^5 Hz. EIS was recorded in conventional 3-electrode system where MSLB over gold behave as working electrode, Ag/AgCl (1 M KCl) as reference electrode and Pt wire as counter electrode.

View Article Online
DOI: 10.1039/D6TB00152A

i.e., from 4.2×10^{-5} F to 4×10^{-6} F upon bilayer assembly (red circle), indicating, consistent with previous reports on pore supported DOPC membrane.[38] For quantitative analysis, the best fits to the experimental curves are obtained using the equivalent circuit model (ECM) shown in the inset of Figure 5a. A representative fitted data to Nyquist and complex capacitance plot corresponding to DOPC bilayer is shown in solid black lines in both panels of Figure 5 a and b.

The absolute magnitude of DOPC membrane resistance (R_M) and capacitance (Q_M) were measured as 4.7 MΩ and 4.8 μFs^{m-1} respectively. Note that these values are not normalized to electroactive area of the working electrode. Also, in the ECM circuit, the introduction of a constant phase element ($CPE=1/Q(j\omega)^m$) rather than a pure capacitor element yielded a better fit; where Q is analogous to the magnitude of the capacitance (C), ω is the angular frequency expressed in rad/s, and m is a CPE exponent real number (~0.94±0.01). While the expression $C_M(\omega)=Q_M\ \omega^{m-1}$ can be used to estimate true membrane capacitance (C_M) from the Q_M value, it only holds true for a specific ω, limited to the specific ECM, and thus is not used in this work. Nonetheless, when normalized to the actual electroactive surface area, the absolute membrane resistance (R_M) and capacitance (C_M) were found to be in the ranges of 15-40 $M\Omega cm^2$ and 0.7-0.9 μFcm^{-2}, respectively. These values are as expected for a highly insulating defect free bilayer and range within previously reported values.[38,55–58] We employ here the relative change in membrane resistance (ΔR) and membrane capacitance (ΔQ) values induced by PLA_2 binding to the membrane, as the absolute values vary depending on electrode area and uniformity of pore packing. ΔR is defined as $R_M^{PLA2} - R_M^0$, where R_M^{PLA2} and R_M^0 are the membrane resistances in the presence and absence of PLA_2. Likewise, ΔQ is defined as $Q_M^{PLA2} - Q_M^0$.

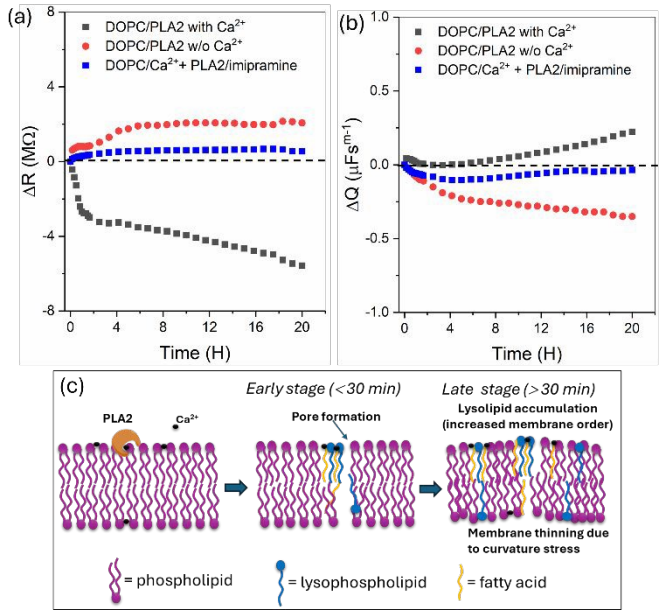

Fig. 6 PLA_2 induced relative change in membrane (a) resistance and (b) capacitance of DOPC MSLB in the absence (red) and presence (black) of 5 mM Ca^{2+} in the contact Tris-HCl buffer. The Blue data in both panels are the trend of resistance and capacitance change of DOPC MSLB induced by pre-incubated 5 μM PLA_2 with 20 μM imipramine. All data points are the average of triplicates under identical experimental conditions. (c) A mechanistic view of nanoporation and increase in membrane order as a result of phospholipid hydrolysis by PLA_2.

Figure 6 a and b shows temporal evolution of relative resistance and capacitance of DOPC MSLB induced by PLA_2 in absence and presence of 5 mM Ca^{2+} respectively. Prior to PLA_2, the relative change in membrane resistance and capacitance over a 20h experimental window is stable, as indicated by the horizontal dotted line near to the origin of Y-axes of Figure 6a and b. Without Ca^{2+}, upon addition of PLA_2, the membrane resistance increases and stabilizes within 4-6 hours (red filled circle, Figure 6a). Correspondingly, capacitance decreased and saturates out within the same time window, (Figure 6b). Since capacitance (C) is inversely related to the thickness (d) of bilayer membrane according to Eq. (3);

$$C = \varepsilon\varepsilon_0 A/d \qquad (3)$$

where ϵ is vacuum permittivity, ε_0 is dielectric constant and A is the electrode area over which bilayer is spanned, this suggests that the membrane is thickening, likely due to PLA_2 adsorption to the bilayer. In presence of 5 mM Ca^{2+}, PLA_2 elicited a rapid drop in membrane resistance that stabilised within an 1h. Beyond this time, a modest but systematic decrease in resistance was evident (black filled square, Figure 6a). This is consistent with the findings of Bilewicz et al. who observed a decrease in charge transfer resistance of a hybrid tethered dodecanethiol-DPPC:cholesterol bilayer on PLA_2 binding.[59] The corresponding capacitance data showed no change up to 5h whereafter the capacitance increased modestly with time. A decrease in resistance without accompanying changes to capacitance suggests nanopore-formation and the subsequent increase in capacitance is taken to be due to membrane thinning, consistent with the study reported by Jenkins et al. at a tethered bilayer platform comprised of complex lipid composition.[60]

Considering the increased membrane viscosity reflected in FCS and Laurdan studies vide infra, it was expected that PLA_2 hydrolysis might manifest increased membrane resistance. However, our real-time EIS experiments, reveal a dynamic response that reflects a more heterogeneous system: At the early-stage of enzyme incubation pore formation predominates, while at later stages extensive membrane organization occurs. We believed that the hydrolytic reaction proceeds, the products (lysophospholipid and fatty acid) form more tightly packed structures within the membrane, potentially forming domains, aligned with FCS and Laurdan fluorescence data; however, due to the inverted-cone morphology of lysophospholipid compared to the cylindrical structure of phospholipid, the former induces positive curvature, resulting in membrane thinning (resistance decrease) at a later stage, as evidenced by our EIS data and schematically illustrated in Fig. 6c. Further evidence of nanopore formation within pore-suspended DOPC lipid bilayers was obtained in analogous PDMS based MSLB platform using confocal imaging, where water soluble membrane impermeable dye, pyranine, was introduced to the aqueous filled cavities prior to bilayer assembly and imaged under confocal microscope (Fig. S8, SI), confirming the pristine DOPC

View Article Online
DOI: 10.1039/D6TB00153A

membrane is intact and impermeable to pyranine. Following addition of PLA_2 in presence of Ca^{2+}, extensive pyranine leakage was evident, confirming pore formation without the loss of membrane integrity.[61]

Imipramine inhibits the PLA_2 enzymatic effect, reflected in a modest overall increase in resistance (blue filled square, Figure 6a) and decrease in capacitance (blue, Figure 6b) when PLA_2 is pre-incubated with 20 µM imipramine drug before treatment of DOPC MSLB in Ca^{2+} containing buffer. The pre-incubation with imipramine may either alter PLA_2 conformation or blocks the catalytic active sites of the PLA_2 enzyme.[62] Our EIS data indicates weak physisorption of PLA_2 to the membrane's surface when PLA_2 is pre-incubated with the imipramine, which supports the modest decrease in lipid diffusivity as discussed earlier.

3.5 Atomic force microscopy studies of lipid hydrolysis using PLA_2

To understand topographic changes to the membrane on PLA_2 interaction, in particular to validate pore formation, which is difficult to resolve by fluorescence imaging, atomic force microscopy imaging was carried out on DOPC planar supported lipid bilayer (SLB) membrane, in this case over freshly cleaved mica substrate under buffer.

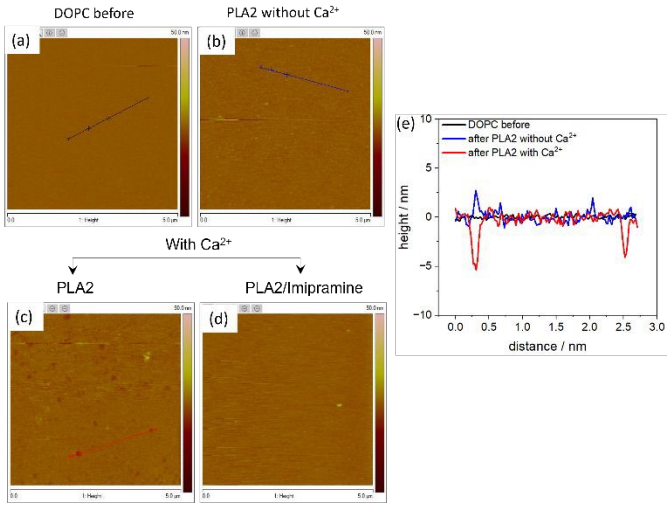

Fig. 7 Topographic AFM images of DOPC lipid bilayer (a) without and (b) with presence of PLA_2 in the absence of Ca^{2+} supported over mica substrate. Panel (c) represents the AFM image of DOPC bilayer in presence of 5 mM Ca^{2+} after incubation with PLA_2. Panel (d) represents the AFM image of DOPC MSLB after incubation of imipramine treated PLA_2 in presence of Ca^{2+}. Panel e illustrates the line profile analyses obtained from the region of interest as indicated by line in panel a-c. All imaging was carried out under Tris-HCl buffer of pH 7.4. The image size was 5 µm×5µm.

We selected SLB for the AFM research rather than MSLB as the atomically smooth solid support facilitates resolution of nanoscale changes caused by protein binding.[53] The DOPC membrane as assembled on mica is homogeneous (Figure 7a) as reflected in the corresponding line profile analysis in panel 7e (black). Following 1h incubation with PLA_2 in absence of Ca^{2+}, the overall membrane remains homogeneous but with occasional appearance of nano protuberances of 2-3 nm height attributed to nanoclusters of PLA_2 (cf. Panel 7e, blue). These results are consistent with the observed decrease in membrane admittance seen in EIS data. When Ca^{2+} was present in the buffer, PLA_2 induced significant membrane heterogeneity with extensive changes to packing and pore-like features reflected in Figure 7c and the corresponding line profile (red) in Figure 7e. Again, this is consistent with the impedance data that showed decreased impedance of the membrane from EIS confirming the extensive changes to membrane packing and poration indicated by FLCS and EIS data from Ca^{2+} mediated effect of enzymatic action of PLA_2. Again, consistent with our observations, when PLA_2 is pre-incubated with imipramine for 30 minutes before incubation with the membrane, the membrane topography remains homogeneous (Figure 7d). Confirming the enzymatic activity of PLA_2 at the membrane is inhibited by imipramine.

4. Conclusions

In conclusion, we investigated the impact of phospholipase enzymatic activity on triplet–triplet annihilation upconversion (TTA-UC) liposomes. We compared TTA-UC from B2PI–perylene reconstituted in DOPC liposomes in the absence and presence of the enzyme phospholipase A_2 (PLA_2) and with and without Ca^{2+}.

Enzymatic hydrolysis of the DOPC liposomal membrane leads to a systematic reduction in TTA-UC intensity as well as QY with an overall 30-50% decrease in light output. Despite this decline, the upconverted emission remains significant, indicating that liposomal TTA-UC function is preserved even during active enzymatic degradation.

The enzymatic action of PLA_2 is dependent on the presence of Ca^{2+} and in the presence of the competitive inhibitor imipramine, no lipid hydrolysis occurs, and TTA-UC intensity remains indistinguishable from enzyme-free solutions. The decrease in UC intensity is attributed to the impact of enzymatic lipid hydrolysis on the physical properties of the membrane. Our data indicates that it increases lipid packing and decreases membrane fluidity. This is evident in a dramatic reduction in the lipid diffusion coefficient, which decreased from 10.1 ± 0.2 to 1.4 ± 0.3 $\mu m^2 s^{-1}$ upon enzyme mediated hydrolysis. These changes are attributed to the accumulation of hydrolytic products, specifically lysolipids and fatty acids in the liposome membrane as well as adsorption of the PLA2 at the membrane interface.

The impact of enzymatic activity was further confirmed using label-free EIS analysis, where Ca^{2+}-mediated PLA_2 activity increases membrane admittance, whereas in the absence of Ca^{2+} or in imipramine-treated PLA_2 in the presence of Ca^{2+}, membrane admittance decreases. The decrease in membrane admittance is attributed to PLA_2 physisorption at the membrane surface in the absence of hydrolysis. Whereas active hydrolysis resulted in widespread membrane reorganisation and increased admittance due to poration, facilitating easier ion transfer across the bilayer, enzymolysis enhanced membrane admittance. This finding was supported by topographic imaging by AFM.

Overall, this study shows that while diminished, TTA-UC remains efficient following phospholipase enzymatic action on DOPC liposomes. The reduction in efficiency is attributed to increases in viscosity of the membrane that reduces the

collision frequency essential between sensitizer and annihilator. indicate that liposomal TTA-UC, although dye partitioning into different phase domains may play a role. Nonetheless, the data confirms that DOPC TA-UC liposomal systems are robust enough for in vivo applications and this approach may also provide a vehicle for developing logic-gated TTA-UC systems for targeted drug delivery and high-resolution bioimaging where endogenous enzymes are present. Given that DOPC liposomes are homogenously LD phase, it is likely this composition is representative of the most vulnerable liposome formulation so we believe that observations are likely true more broadly for other liposome compositions but this is something that will be investigated In future studies,

Author Contributions

Amrutha Prabhakaran: methodology, formal analysis, methodology, writing – review & editing, investigation. Nirod Kumar Sarangi: conceptualization, methodology, formal analysis, writing – original draft, writing – review & editing, investigation. Colm Smith: methodology, formal analysis, writing – review & editing. Ruben Arturo Arellano Reyes: methodology, formal analysis. Tia E. Keyes: resources, methodology, formal analysis supervision, funding acquisition, writing – review & editing

Conflicts of interest

There are no conflicts to declare.

Data availability

The datasets used and/or analyzed in the current study are available from the corresponding authors upon reasonable request. Supplementary information is available. See DOI:

Acknowledgements

Authors acknowledge European Union's Horizon 2020 research and innovation programme under the Marie Skłodowska-Curie grant agreement No 813920 LogicLab and Taighde Éireann – Research Ireland under Grant Nos. 12/RC/2289_P2 and 19/FFP/6428.

References

1 T. N. Singh-Rachford and F. N. Castellano, *Coord. Chem. Rev.*, 2010, **254**, 2560–2573.

2 H.-J. Feng, M.-Y. Zhang, L.-H. Jiang, L. Huang and D.-W. Pang, *Acc. Chem. Res.*, DOI:10.1021/acs.accounts.5c00403.

3 C. Ye, L. Zhou, X. Wang and Z. Liang, *Physical Chemistry Chemical Physics*, 2016, **18**, 10818–10835.

4 R. A. Arellano-Reyes, A. Prabhakaran, R. C. E. Sia, J. Guthmuller, K. K. Jha, T. Yang, B. Dietzek-Ivanšić, V. McKee and T. E. Keyes, *Chemistry – A European Journal*, DOI:10.1002/chem.202300239.

5 A. Prabhakaran, K. K. Jha, R. C. E. Sia, R. A. Arellano Reyes, N. K. Sarangi, M. Kogut, J. Guthmuller, J. Czub, B. Dietzek-Ivanšić and T. E. Keyes, *ACS Appl. Mater. Interfaces*, 2024, **16**, 29324–29337.

6 W. Wu, H. Guo, W. Wu, S. Ji and J. Zhao, *J. Org. Chem.*, 2011, **76**, 7056–7064.

7 K. Kumar Jha, A. Prabhakaran, R. Cane Sia, R. A. Arellano Reyes, N. Kumar Sarangi, T. Yang, K. Kumar, S. Kupfer, J. Guthmuller, T. E. Keyes and B. Dietzek-Ivanšić, *ChemPhotoChem*, DOI:10.1002/cptc.202300073.

8 P. Bharmoria, H. Bildirir and K. Moth-Poulsen, *Chem. Soc. Rev.*, 2020, **49**, 6529–6554.

9 K. K. Jha, A. Prabhakaran, C. S. Burke, M. Schulze, U. S. Schubert, T. E. Keyes, M. Jäger and B. D. Ivanšić, *Journal of Physical Chemistry C*, DOI:10.1021/acs.jpcc.1c09897.

10 Y. Hou, Z. Zhou, K. Huang, H. Yang and G. Han, *ChemPhotoChem*, 2018, **2**, 1005–1011.

11 S. Askes, M. Meijer, T. Bouwens, I. Landman and S. Bonnet, *Molecules*, 2016, **21**, 1460.

12 W. Wang, Q. Liu, C. Zhan, A. Barhoumi, T. Yang, R. G. Wylie, P. A. Armstrong and D. S. Kohane, *Nano Lett.*, 2015, **15**, 6332–6338.

13 L. Huang, Y. Zhao, H. Zhang, K. Huang, J. Yang and G. Han, *Angewandte Chemie*, 2017, **129**, 14592–14596.

14 A. Prabhakaran, K. K. Jha, R. C. E. Sia, M. Kogut, J. Czub, J. Guthmuller, C. Smith, C. S. Burke, B. Dietzek-Ivanšić and T. E. Keyes, *J. Phys. Chem. B*, 2025, **129**, 6220–6232.

15 S. H. C. Askes, N. L. Mora, R. Harkes, R. I. Koning, B. Koster, T. Schmidt, A. Kros and S. Bonnet, *Chemical Communications*, 2015, **51**, 9137–9140.

16 M. Poznik, U. Faltermeier, B. Dick and B. König, *RSC Adv.*, 2016, **6**, 41947–41950.

17 H. L. Verrill, N. A. Pickard and H. D. Gruemer, *Clin. Chem.*, 1977, **23**, 2219–2225.

18 M. Shinitzky and P. Henkart, 1979, pp. 121–147.

19 G. Lenaz, *Biosci. Rep.*, 1987, **7**, 823–837.

20 K. Jørgensen, J. Davidsen and O. G. Mouritsen, *FEBS Lett.*, 2002, **531**, 23–27.

21 Y. Kita, H. Shindou and T. Shimizu, *Biochimica et Biophysica Acta (BBA) - Molecular and Cell Biology of Lipids*, 2019, **1864**, 838–845.

22 R. H. Schaloske and E. A. Dennis, *Biochimica et Biophysica Acta (BBA) - Molecular and Cell Biology of Lipids*, 2006, **1761**, 1246–1259.

23 E. A. Dennis, J. Cao, Y.-H. Hsu, V. Magrioti and G. Kokotos, *Chem. Rev.*, 2011, **111**, 6130–6185.

24 M. Menschikowski, A. Hagelgans, B. Nacke, C. Jandeck, O. A. Mareninova, L. Asatryan and G. Siegert, *Tumor Biology*, 2016, **37**, 8097–8105.

25 X. Wang, C.-J. Huang, G.-Z. Yu, J.-J. Wang, R. Wang, Y.-M. Li and Q. Wu, *Hum. Pathol.*, 2013, **44**, 2020–2027.

26 T. MIRTTI, V. J. O. LAINE, H. HIEKKANEN, S. HURME, O. ROWE, T. J. NEVALAINEN, M. KALLAJOKI and K. ALANEN, *APMIS*, 2009, **117**, 151–161.

27 T. Andresen, S. Jensen, T. Kaasgaard and K. Jorgensen, *Curr. Drug Deliv.*, 2005, **2**, 353–362.

28 T. L. Andresen, J. Davidsen, M. Begtrup, O. G. Mouritsen and K. Jørgensen, *J. Med. Chem.*, 2004, **47**, 1694–1703.

29 H. Kapalatiya, Y. Madav, V. S. Tambe and S. Wairkar, *Drug Deliv. Transl. Res.*, 2022, **12**, 1293–1305.

30 H. Alrbyawi, I. Poudel, M. Annaji, R. D. Arnold, A. K. Tiwari and R. J. Babu, *Pharm. Nanotechnol.*, 2022, **10**, 3–23.

31 G. B. Berselli, N. K. Sarangi, A. V. Gimenez, P. V. Murphy and T. E. Keyes, *Chemical Communications*, 2020, **56**, 11251–11254.

32 A. Roy, N. K. Sarangi, S. Ghosh, A. Prabhakaran and T. E. Keyes, *J. Phys. Chem. Lett.*, 2023, **14**, 3920–3928.

33 A. V. Gimenez, K. W. Kho and T. E. Keyes, *Nanoscale Adv.*, 2020, **2**, 4740–4756.

34 B. Radwan, A. Prabhakaran, S. Rocchetti, E. Matuszyk, T. E. Keyes and M. Baranska, *Microchimica Acta*, DOI:10.1007/s00604-023-05888-8.

35 D. M. Klein, S. Rodríguez-Jiménez, M. E. Hoefnagel, A. Pannwitz, A. Prabhakaran, M. A. Siegler, T. E. Keyes, E. Reisner, A. M. Brouwer and S. Bonnet, *Chemistry - A European Journal*, DOI:10.1002/chem.202102989.

36 N. K. Sarangi, A. Stalcup and T. E. Keyes, *ChemElectroChem*, 2020, **7**, 4535–4542.

37 N. K. Sarangi, A. Prabhakaran and T. E. Keyes, *Electroanalysis*, DOI:10.1002/elan.202060424.

38 N. K. Sarangi, A. Prabhakaran and T. E. Keyes, *Langmuir*, DOI:10.1021/acs.langmuir.2c00524.

39 N. K. Sarangi, A. Prabhakaran, M. Roantree and T. E. Keyes, *Colloids Surf. B Biointerfaces*, DOI:10.1016/j.colsurfb.2023.113688.

View Article Online
DOI: 10.1039/D6TB00152A

40 N. K. Sarangi, N. Ramesh and A. Patnaik, *J. Chem. Phys.*, DOI:10.1063/1.4905075.

41 H. Cai, E. G. Chiorean, M. V. Chiorean, D. K. Rex, B. W. Robb, N. M. Hahn, Z. Liu, P. J. Loehrer, M. L. Harrison and Y. Xu, *PLoS One*, 2013, **8**, e57081.

42 R. M. Kramer and J. D. Sharp, *FEBS Lett.*, 1997, **410**, 49–53.

43 L.-S. Chang, S.-R. Lin and C.-C. Chang, *J. Protein Chem.*, 1996, **15**, 701–707.

44 X. Zhang, D. S. Alves, J. Lou, S. D. Hill, F. N. Barrera and M. D. Best, *Chemical Communications*, 2018, **54**, 6169–6172.

45 M. N. Holme, M. H. Rashid, M. R. Thomas, H. M. G. Barriga, K. Herpoldt, R. K. Heenan, C. A. Dreiss, J. L. Bañuelos, H. Xie, I. Yarovsky and M. M. Stevens, *ACS Cent. Sci.*, 2018, **4**, 1023–1030.

46 J. Lou and M. D. Best, *Chemistry – A European Journal*, 2020, **26**, 8597–8607.

47 S. Ramadurai, N. K. Sarangi, S. Maher, N. MacConnell, A. M. Bond, D. McDaid, D. Flynn and T. E. Keyes, *Langmuir*, 2019, **35**, 8095–8109.

48 J. H. Evans, S. H. Gerber, D. Murray and C. C. Leslie, *Mol. Biol. Cell*, 2004, **15**, 371–383.

49 M. S. Hixon, A. Ball and M. H. Gelb, *Biochemistry*, 1998, **37**, 8516–8526.

50 C. Leidy, J. Ocampo, L. Duelund, O. G. Mouritsen, K. Jørgensen and G. H. Peters, *Biophys. J.*, 2011, **101**, 90–99.

51 N. K. Sarangi, S. Mondal and T. E. Keyes, *Biophys. Chem.*, 2025, **322**, 107441.

52 J. Robinson, N. K. Sarangi and T. E. Keyes, *Physical Chemistry Chemical Physics*, 2023, **25**, 7648–7661.

53 N. K. Sarangi, M. Shafaq-Zadah, G. B. Berselli, J. Robinson, E. Dransart, A. Di Cicco, D. Lévy, L. Johannes and T. E. Keyes, *J. Phys. Chem. B*, 2022, **126**, 10000–10017.

54 A. Roy, S. Byrne, N. K. Sarangi, P. V. Murphy and T. E. Keyes, *Front. Mol. Biosci.*, DOI:10.3389/fmolb.2022.1017338.

55 G. Wiegand, N. Arribas-Layton, H. Hillebrandt, E. Sackmann and P. Wagner, *J. Phys. Chem. B*, 2002, **106**, 4245–4254.

56 F. Abbasi, J. J. Leitch, Z. Su, G. Szymanski and J. Lipkowski, *Electrochim. Acta*, 2018, **267**, 195–205.

57 M. S. Khan, N. S. Dosoky, B. K. Berdiev and J. D. Williams, *European Biophysics Journal*, 2016, **45**, 843–852.

58 P. C. Gufler, D. Pum, U. B. Sleytr and B. Schuster, *Biochimica et Biophysica Acta (BBA) - Biomembranes*, 2004, **1661**, 154–165.

59 A. Więckowska, E. Jabłonowska, E. Rogalska and R. Bilewicz, *Physical Chemistry Chemical Physics*, 2011, **13**, 9716.

60 T. N. Tun and A. T. A. Jenkins, *Electrochem. commun.*, 2010, **12**, 1411–1415.

61 R. Georgieva, K. Mircheva, V. Vitkova, K. Balashev, T. Ivanova, C. Tessier, K. Koumanov, P. Nuss, A. Momchilova and G. Staneva, *Langmuir*, 2016, **32**, 1756–1770.

62 K. Kucia, A. Małecki, B. Gabryel and H. I. Trzeciak, *Pol. J. Pharmacol.*, 2003, **55**, 5–15.

View Article Online
DOI: 10.1039/D6TB00152A

View Article Online
DOI: 10.1039/D6TB00152A

The data supporting this article have been included as part of the supplementary information (SI).

The following datasets are available to researchers upon request to the authors:

- Electrochemical Impedance Data.
- Fluorescence Decay Data
- Fluorescence Correlation Data